Development of a Novel Test Setup for Validation of Virtual Sensing on Mechatronic Drivetrains

B. Forrier [1], R. Boonen, and W. Desmet [1]

Department of Mechanical Engineering, KU Leuven, Leuven, Belgium
[1] Member of Flanders Make

Abstract: This paper discusses the design of a novel mechatronic drivetrain test setup. The primary goal of this test setup is to experimentally validate model-based virtual sensing on an electro-mechanical drivetrain with nonlinear torsional dynamics. Its layout, instrumentation and design requirements are focused on dynamic load torque estimation using online coupled state and input estimators. The proposed driveline primarily consists of two induction machines in back-to-back, coupled by a double cardan transmission in Z-configuration. The main novelty of the test setup is that the extent of nonlinearity in the torsional driveline dynamic behaviour can be tuned by altering this Z-configuration. The required modelling and identification effort is limited by decoupling the frame dynamics from those of the driveline. The result is a mechatronic drivetrain with torsional dynamic behaviour that can be dominated by a tuneable amount of cardan-induced nonlinear effects and modelled with disregard of the frame. These features will be useful for validation of model-based virtual sensors.

Keywords— design, mechatronic, torque estimation, virtual sensing

1-Introduction

Mechatronic drivetrains are ever more present in vehicles, energy conversion systems and industrial machinery. As conception and use of such systems evolves towards light-weight design and high dynamic operation, the mechanical dynamics interact with the electric supply at the motor or generator. This influences the operational loading in applications like wind turbines [1] and can be used to improve vehicle noise, vibration and harshness performance [2]. Detailed knowledge and improvement of mechatronic drivetrain performance thus requires insight in their operational dynamic behaviour. Knowledge of torsional loads is very useful for this purpose. However, direct torque measurements are expensive and often impossible due to their intrusive character.

Some previous work has therefore been aimed at indirect torque measurement. A virtual sensing approach for dynamic load torque estimation has been developed and numerically validated [3]. This approach embeds a nonlinear electro-mechanical torsional driveline model in an Unscented Kalman Filter (UKF) scheme [4,5]. An a priori unknown input torque acts on one side of the modelled driveline. The online executable recursive algorithm then consists of a model-based prediction step, followed by a measurement-based correction of the system states and the a-priori unknown torque. The proposed combination of electrical and mechanical measurements provides a reliable load torque estimate in the frequency band of 0 Hz to 200 Hz.

This paper describes the design of a novel test setup to experimentally validate this virtual load torque sensing approach and other [6] research results in the context of driveline dynamics and the extended use of models throughout the operational life of mechatronic systems. A setup will be proposed such that nonlinear model-based state and input estimation can be validated experimentally in a wide range of operating conditions. Its design will therefore allow to tune the extent of driveline nonlinearity and ensure that these nonlinear dynamics can be modelled.

Section 2 explains the translation of the test setup's purpose into functional requirements. Section 3 then provides an overview on the final result in terms of electrical, mechanical, control and instrumentation layout. Section 4 focuses on the mechanical driveline design and section 5 provides insight in how the frame and its suspension are designed. Finally, section 6 validates the design approach by means of preliminary measurement data.

2-Specification of Requirements

The main purpose of the test setup is to provide a platform for experimental validation of newly developed model-based online load torque estimation approaches. The related basic research is focused on drivelines with nonlinear electrical and mechanical dynamics [3]. Table 1 lists the functional requirements that follow from this purpose and contribute to the novelty of the setup.

A first requirement for the test setup is to include a nonlinear driveline element. As experimental load torque estimation will require an accurate torsional driveline model, the nonlinear relation between applied input torque and resulting acceleration should be well-defined and predictable. Moreover, in order to assess the influence of relevant nonlinear dynamics on the quality of possible estimation algorithms, one should be able to change the extent of nonlinearity in a convenient manner on the real driveline and on its virtual counterpart.

Table 1: Functional design requirements.

Requirement	Implications on design
Nonlinear element	Double cardan transmission
Tuneable extent of nonlinearity	Z-configuration, variable offset
Modular driveline	Flange-mounting, telescopic shaft
Predictable driveline dynamics: *Driveline model* adequate to describe torsional dynamics	Precisely defined (Z-) configuration Decoupling from frame dynamics Limited unbalance forces

The test setup should also be instrumental for other research purposes, including unbalance estimation [6]. This is taken into account by requiring a modular layout, in the sense that the torque transfer path can be changed in a couple of minutes.

The first three requirements in Table 1 help define the driveline layout. The following section clarifies this by discussing the final test setup. Sections 4 and 5 explain how the last requirement imposes constraints on the detailed mechanical design of the driveline and frame, respectively.

3-Overview of the final setup

Fig. 1 shows the final computer-aided design (CAD) model, along with an indication of the main driveline components as further specified in Table 2. Both 2-pole 5,5 kW induction machines are flange-mounted and their rotors are mechanically connected by the double-cardan assembly in series with the torque flange and flexible coupling. The flexible coupling allows a small radial and angular misalignment. The set of angular contact ball bearings in O-configuration is preloaded such that clearance is removed [7]. As such, the torque sensor is only subjected to a torsional load and its measurement accuracy is maximized.

Nonlinear driveline behaviour stems from the combination of cardan joints with nonlinear kinematics [8] and linear dynamics of the intermediate shaft. When looked at from the motor or generator side, the constant stiffness and rotational inertia of the intermediate shaft vary periodically as the driveline rotates. This variation repeats itself twice per revolution and increases as the offset between in- and outgoing shaft increases. Torsional vibrations arise as a result, on frequencies corresponding to even harmonics of the shaft frequency. Their amplitude is largest for the second harmonic and decreases for each successive multiple.

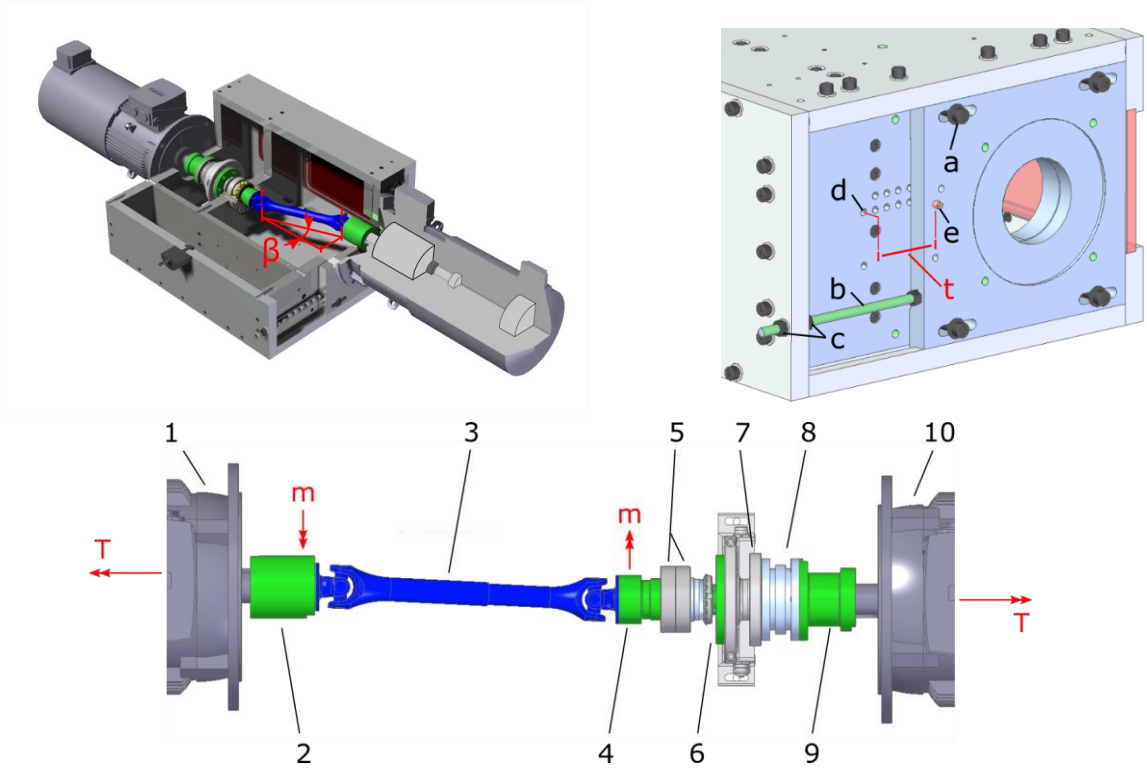

Fig. 1: Final CAD model with indication of driveline components according to Table 2.

Table 2: Main driveline components.

Indication of Fig. 1	Component	Manufacturer and model
1	Motor	Siemens 3-phase squirrel-cage-motor model 1LE1001-1CA02-1FH4-Z
2	Adapter-Motor	In-house design
3	Double-cardan assembly	ELBE (distributed by Voight) Model ST-058.1S58R300
4	Adapter-Bearing	In-house design
5	Set of bearings (O-configuration)	SKF 7208 angular contact ball bearings for universal matching
6	Adapter-Sensor	In-house design
7	Torque sensor	HBM T40B 50 Nm Torque flange
8	Flexible coupling	Mayr Roba-DS Lamellae coupling
9	Adapter-Generator	In-house design
10	Generator	Siemens 3-phase squirrel-cage-motor model 1LE1001-1CA02-1FH4-Z

The design of Fig. 1 allows to evoke this nonlinear torsional dynamic effect by displacing the motor laterally with respect to the generator. Translating the motor is practically possible by fixing the motor flange to a vertical plate which slides left-to-right as indicated in the top-right of Fig. 1. During operation, the plate is tightly connected to the rest of the frame through four M12 screws (a). Positioning requires removing these screws and rotating screw nuts (c) around the fine-threaded rod (b), thus exerting a lateral pulling or pushing force on the plate until the required offset (t) is reached. The positioning can then be checked using a set of precisely drilled bores (d) in which an alignment pin (e) is fitted. The corresponding cardan joint deflection angle β is related to the lateral offset t in [mm] by the geometric relation (1):

$$\tan(\beta) = t/240 \tag{1}$$

Fig. 2 illustrates how the frame with driveline is integrated in the complete test setup. As indicated in this figure, the user provides inputs such as a reference generator torque and motor speed. Practically, this happens through a rapid control prototyping (RCP) platform supplied by Triphase. This platform enables the user to build a control model in Matlab-Simulink, after which it is compiled and run on the real-time target (RTT). The control algorithm provides a set of reference line duty cycles. The inverters translate these duty cycle inputs into power transmission by means of pulse-width modulated (PWM) motor line voltage supplies.

As both inverters are supplied by a common DC-bus, four-quadrant operation is supported. The addition of braking resistors (BR) avoids overloading the DC-bus under heavy braking. The result is a power and control scheme which covers a wide range of regime and transient operating conditions in the range of -5,5 to +5,5 kW and -3000 to +3000 rpm. The user can specify torque and speed reference values, or arbitrarily shaped time-varying reference profiles.

Fig. 2 also indicates the available instrumentation. This includes 1024-pulse incremental quadrature encoders and ACC74 Ferraris rotational acceleration sensors [9] at both extremities of the driveline and the torque sensor between generator and cardan assembly. Each induction machine is instrumented with three PT100 temperature sensors, one per stator phase winding. On the electrical side, terminal currents are measured on the generator and terminal phase voltages and currents on the motor. All these signals are captured synchronously on the RTT and processed using the Matlab-Simulink control model. They can also be stored for further processing on the engineering pc.

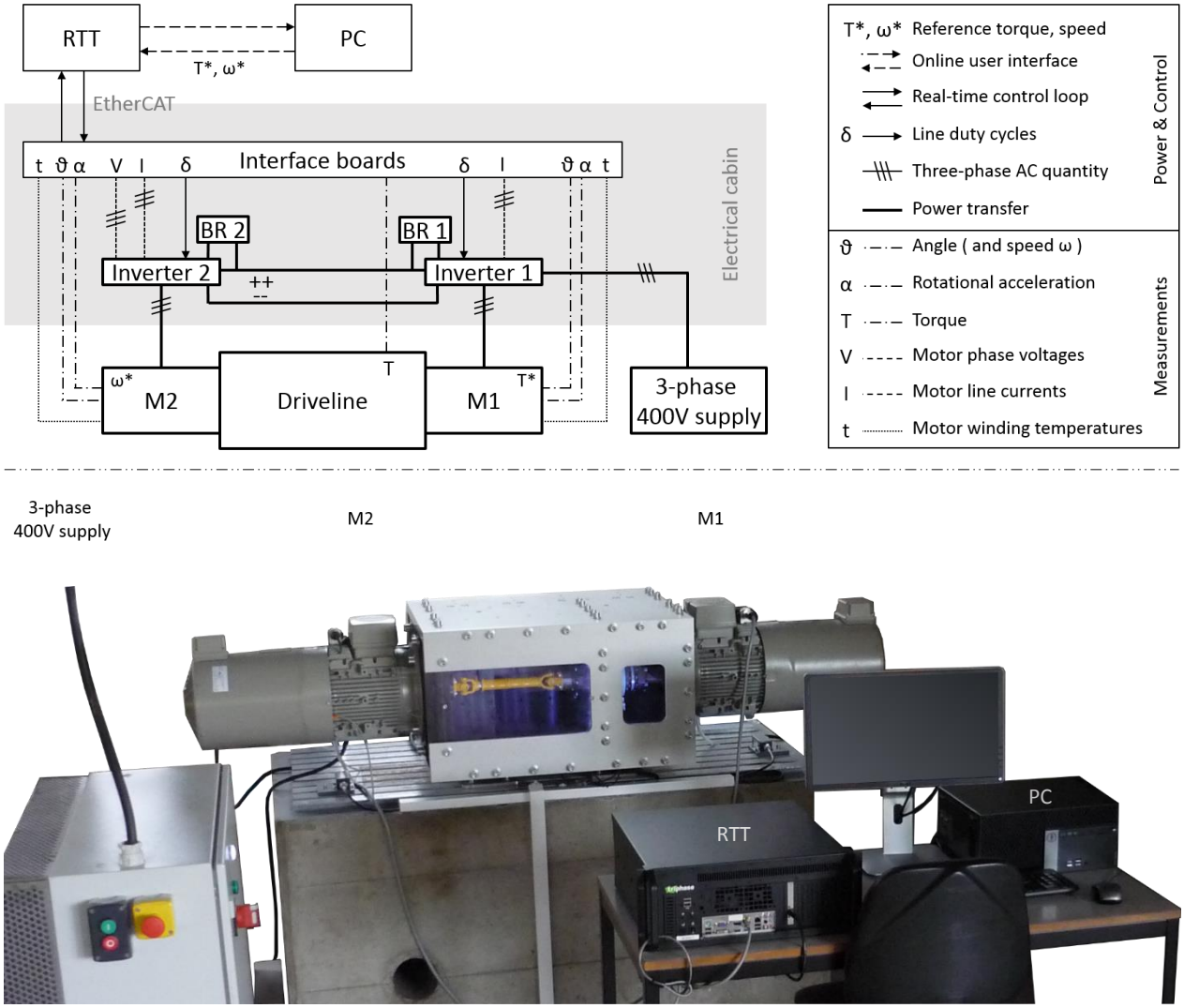

Fig. 2: Schematic and actual overview of the test setup.

4-Driveline design

Fig. 3 shows the main in-house designed driveline components (cfr. Fig. 1, Table 2). Each component transmits torque through a friction flange at one end and a keyway with key at the other end. The user imposes torsional loads without directly controlling them. Because of this and the possible replacement of the cardan assembly by other components, the applied load is highly uncertain. The considered static and dynamic loading therefore assumes the following:

- Components are subject to a pulsating torsional load;
- The double-cardan assembly is mounted in Z-configuration with maximal offset;
- The maximum applied static torque equals the induction machines' breakdown torque;
- The maximum applied dynamic torque equals the machines' nominal torque.

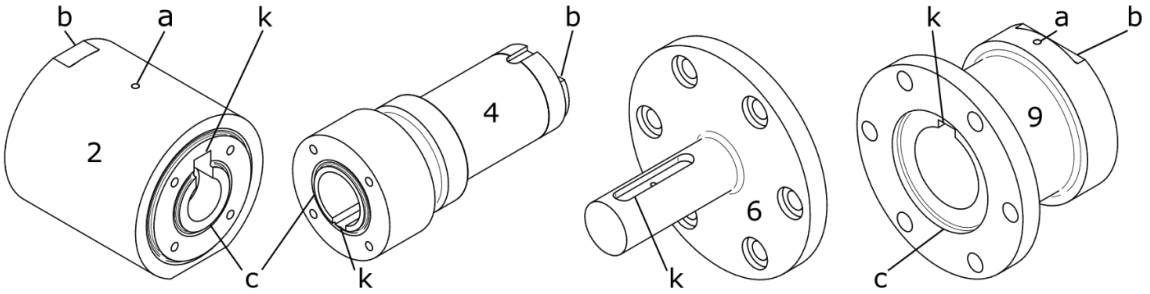

(a) (b) (c) (d)

Fig. 3: Driveline components with threaded holes for axial fixation (a), balancing cut-outs (b), centering rings (c) and keyways (k).

The first assumption stems from the knowledge that torsional driveline resonance phenomena and cardan-induced torsional vibrations are periodic. These will be superposed onto a user-defined constant load torque, such that zero-crossings are avoided. The dimensioning of keys and keyways takes this into account according to the DIN 6885 standard [10].

When applying a constant torque T on a cardan assembly with nonzero deflection angle β, the latter exerts a bending moment m on both sides of the driveline. This bending load is illustrated in Fig. 1 and pulsates twice per revolution [11]. Its maximum value M is related to the deflection angle β by (2). In this equation, the maximum deflection angle of (3) is used.

$$M = T.\tan(\beta) \tag{2}$$

$$\tan(\beta_{max}) = 100/240 \tag{3}$$

Based on forementioned assumptions, both a static and dynamic component stress evaluation is performed. For dynamic stress calculations, the nominal torque value is multiplied by an application factor of 1.4 according to the standardized mechanical engineering practice [12] which follows the DIN 3990 standard [13]. In this case, stress calculations assume the bending load with maximum value M to be alternating instead of pulsating. This is done to allow safe replacement of the cardan assembly by a driveline mainly loaded by unbalance.

The torsion- and bending-induced mechanical stresses are combined according to the Von Mises distortion energy theory (DET), taking into account stress concentrations [12]. The most important geometric features that lead to such stress concentrations are shown in Fig. 3:

- All four components have at least one axial variation of inner or outer diameter size;
- All four components have a keyway (component 6 has a keyway with ends);
- Components 2, 6 and 9 have a threaded hole for axial fixation;
- Components 2 and 9 have balancing cut-outs.

The goal of the balancing cut-outs in Fig. 3 is to limit the parasitic effect of unbalance in terms of e.g. torque and speed ripple amplitudes. As such the driveline behaviour is dominated by the parallel misalignment of the cardan assembly. These cut-outs are therefore dimensioned so that each component is balanced up to grade G2,5 for 3000 rpm, according to the half-key method as specified in the ISO 1940-1:2013 standard [14].

5-Frame design

The frame's primary function is to precisely define the driveline configuration. This is partly ensured by the stiff bearing arrangement and flange-mounting of both induction machines. However, the frame itself should also form a rigid entity throughout the machine's operating region. Only then, the driveline dynamics can be predicted without modelling the frame. The latter's dynamic stiffness should thus be sufficiently high such that frame resonances are above the excited frequency range.

The resulting engineering criterion is therefore formulated in terms of eigenfrequencies as follows. The starting point is the acceleration of the intermediate shaft in the double-cardan assembly [8], assuming the motor to rotate at a constant speed of 3000 rpm. Fig. 4 shows this acceleration in the time and frequency domain for three possible lateral motor offset values. The second shaft order frequency is dominant as expected, with growing amplitudes of even harmonics as the offset value is increased. Torsional and bending excitation of the frame would be proportional to these acceleration spectra in the case of a rigid driveline. The first torsional driveline resonance is estimated well below 100 Hz, based on manufacturer data of the different driveline components. The actual frame excitation in the frequency region above 100 Hz is therefore expected to be lower than suggested by the spectra of Fig. 4. The overlaid frequency response function (FRF) is proportional to deformation of a frame with its first eigenfrequency at 400 Hz. The driveline dynamics are then well decoupled from the frame dynamics, except for the 8^{th} order harmonic in the extreme, practically not allowed [11] case of maximal speed and offset. Up to the dominant excitation component at 100 Hz, the frame dynamics are irrelevant as they should be. The frame's stiffness criterion is therefore specified as having its first deformation mode at a natural frequency of at least 400 Hz.

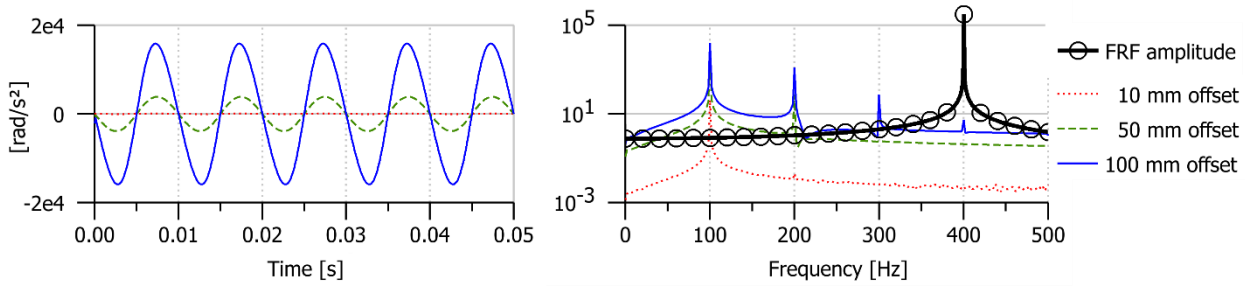

(a) (b)

Fig. 4: Intermediate shaft acceleration for a constant motor speed of 3000 rpm: (a) time signal and (b) amplitude spectrum for three lateral offset values, overlaid with a displacement FRF amplitude for a system with one eigenmode at 400 Hz and 2 percent modal damping.

Fig. 5 illustrates the iterative design procedure followed to reach this stiffness criterion. This procedure makes use of MSC.Patran as pre-processor to generate the finite element (FE) model of the frame assembly and to formulate the numerical modal analysis (MA) as an orthogonal eigenvalue problem [15]. The solver MD.Nastran is then employed to compute the five lowest undamped free-free deformation mode shapes and natural frequencies.

The FE model represents the plate assembly by means of quadratic 2D plate elements. The screw connections between these plates are idealized by imposing coincident nodes to have equal displacements. The validity of this assumption is critical in avoiding to overestimate the frame's eigenfrequencies, as stiffness of the individual plates contributes to that of the overall frame only when the connections are stiff as well. It will therefore be verified numerically for the final design and experimentally during construction. Adding the driveline components' mass significantly lowers the natural frequencies of the plate assembly. The induction machines are the main contributors to this effect, hence their masses and centres of gravity should be represented correctly. The driveline deformation is less relevant. Therefore the driveline is modelled by a series of 1D beam elements. It is not assumed to add any stiffness as the cardan assembly is represented by two disconnected shafts. These each represent half of the cardan assembly's mass. The free-free boundary condition is imposed on this FE model, because the frame mass will be suspended on soft rubber bushings with natural frequencies below 6.4 Hz. As such, the frame stiffness will not depend on the stiffness of its mounting points.

The numerical modal analysis translates this FE model into its five lowest undamped free-free deformation mode shapes and frequencies. These are evaluated and design changes are made accordingly, resulting in an updated FE model. This iterative procedure (Fig. 5a) is carried out in two subsequent stages. The first stage updates the general layout of the frame, along with one global plate thickness value. This stage assumes all plates to be made of aluminium. It ends when the lowest eigenfrequency approximates the target value within approximately 15 percent. The second stage updates separate plate thickness values. It also introduces the use of steel plates, by attributing the corresponding mass density and Young's modulus values to a subset of the plate elements. Stage two ends when it reaches the stiffness criterion in the strict sense. Fig. 5b shows the then obtained result: an FE model with specified plate dimensions and materials. The lowest three modes have natural frequencies of 413 Hz, 497 Hz and 502 Hz. The frame's natural frequencies thus exceed 400 Hz for all deformation modes.

Translating this FE model into a detailed design leads to a sufficiently stiff frame, on the condition that the initial modelling assumptions are valid:

- sufficiently stiff plate connections; (C1)
- a sufficiently soft suspension. (C2)

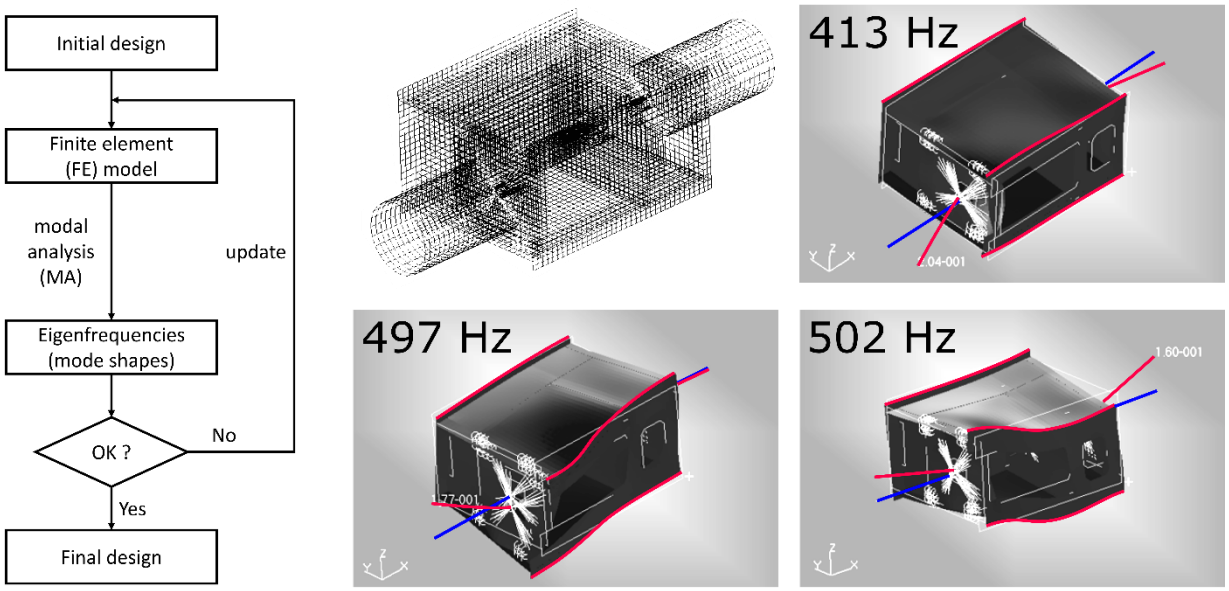

(a) (b)

Fig. 5: Procedure (a) and final result (b) of the frame design according to the stiffness criterion.

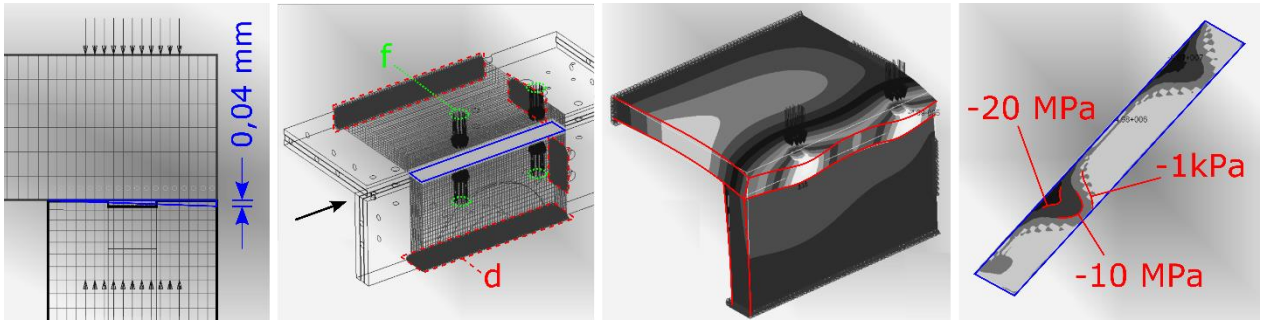

(a) (b) (c) (d)

Fig. 6: FE contact analysis for verifying the assumption of ideal plate connections.

The nonlinear static FE contact analysis of Fig. 6 verifies condition C1. This analysis uses a fine mesh of linear hexahedral elements and penalty-based contact detection. It assumes an initial gap of 0,04 mm at one side of the most critical plate-plate interface (Fig. 6a). This corresponds to the worst case according to manufacturing tolerance specifications. The imposed boundary conditions (Fig. 6b) consist of two sets of screw pretension forces ***f*** and four regions of zero-displacements ***d***. The zero-displacement regions are either far from the interface or close to unmodelled screw connections. The resulting displacement field (Fig. 6c) closes the gap. This is verified by the vertical contact pressure distribution over the interface element faces (Fig. 6d), indicating zones with high contact pressure values and thus a high contact stiffness. The actual design will have 1 mm grooves along all plate edges (see Fig. 6a and Fig. 6b), which further increases the contact stiffness between each set of plates. Condition C1 is thus fulfilled.

Condition C2 is verified by adding linear spring elements to the FE model of Fig. 5. These elements are fixed to the frame at the three actual mounting points (Fig. 7a). Their manufacturer-supplied axial and lateral stiffness values are only valid in a limited deformation range. A static analysis, where both induction machines suddenly exert their breakdown torque on the frame (Fig. 7a), confirms that this linear range is not exceeded. A numerical MA based on the same FE model then yields the six rigid body modes (RBM) and eigenfrequencies. The latter are valued between 1.6 Hz and 6.4 Hz. Since the highest of these frequencies (Fig. 7b) is almost 2 orders of magnitude lower than the lowest free-free deformation mode frequency of 413 Hz, the modelled suspension is sufficiently soft. Condition C2 is thus also fulfilled.

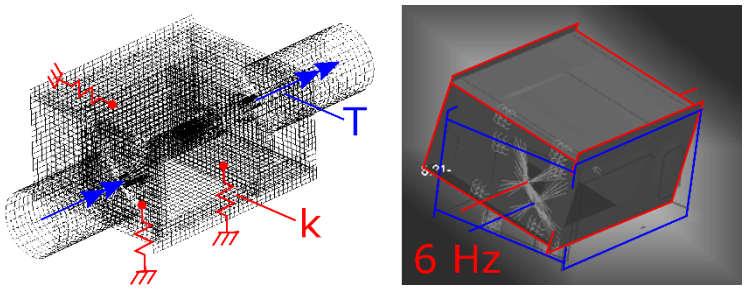

(a) (b)

Fig. 7: (a) FE model with spring elements (k) for RBM computation and additional torques (T) for static displacement analysis. (b) The highest RBM frequency is valued at 6.4 Hz.

6-Measurement-based design validation

Two preliminary measurement campaigns are performed to verify that driveline dynamics can indeed be modelled with disregard of the frame dynamics. The first campaign checks the stiffness of the frame before adding the driveline components. The second campaign verifies the dominant presence of cardan-induced torsional vibrations in the Z-configured driveline.

The frame stiffness is checked directly after having mounted the frame without driveline on the soft bushing elements. This is done by means of an experimental modal analysis (EMA) using the roving-hammer excitation technique [15]. An LMS SCADAS system is used for acquiring the excitation force and response acceleration signals in the frequency domain. LMS Test.Lab is used for the subsequent FRF-based modal identification. These experimental results are compared to a variant of the previously used FE model (Fig. 5b), where the driveline elements have been removed. Fig. 8 shows this for the first two mode shapes and frequencies: a tight correspondence exists between experimental and FE-based results. This supports the contact analysis in validating the ideal plate-to-plate contacts in the FE model of Fig. 5.

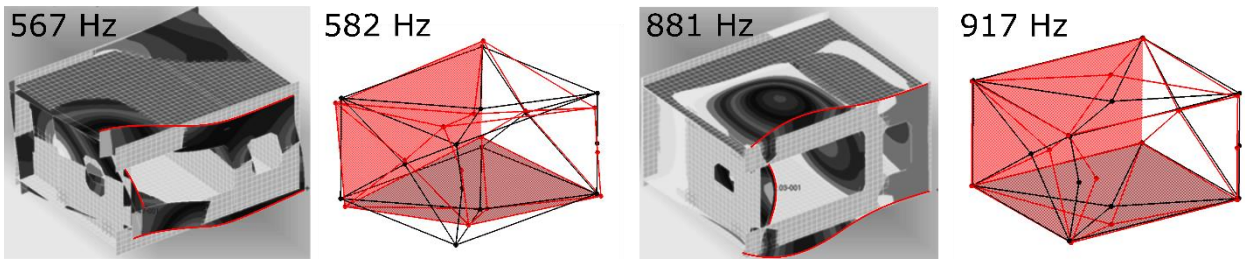

(a) (b) (c) (d)

Fig. 8: First (a-b) and second (c-d) frame deformation modes. Experimental FRF-based eigenfrequencies (b, d) and FE-based results (a, c) correspond to within 4 percent.

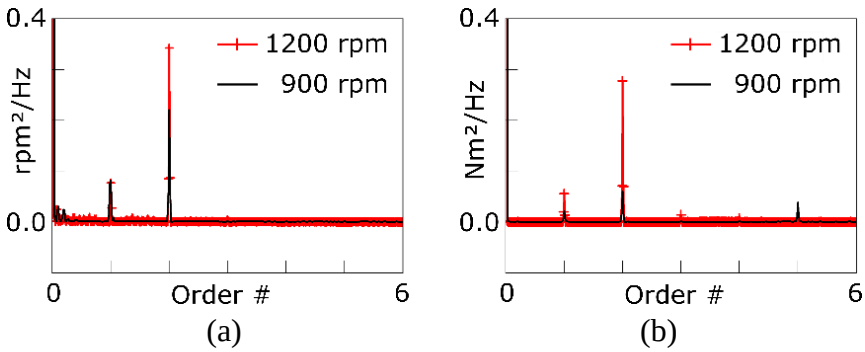

Fig. 9: PSD of measured speed (a) and torque (b) at a lateral motor offset of 60 mm.

After the Z-configured double-cardan driveline is mounted, its operational dynamic behaviour is checked for the case of constant motor speed and generator torque reference values. A signature analysis is performed on the encoder-based speed signal at the generator side and on the HBM torque signal, using LMS Test.Lab to process the time signals into the power spectral densities (PSD) of Fig. 9. Superposed on their 0 Hz components, the speed and torque responses feature a dominant component at twice the generator shaft frequency of rotation. This is as expected for the Z-configured double-cardan assembly. The measured PSD also contain other components, like e.g. a first-order component which is attributed to mechanical unbalance. Their amplitudes are significantly lower than that of the second-order component, as aimed for in the driveline design.

7-Conclusion

A test setup has been designed for the purpose of validating model-based estimation methods, such as online load torque estimation, on mechatronic drivetrains. The result consists of a speed-controlled motor, coupled to a torque-controlled generator by a re-configurable and replaceable double cardan transmission. A design procedure and verification based on FE modelling and modal analysis techniques has ensured a high dynamic frame stiffness. Torsional driveline models for virtual sensing may thus disregard frame dynamics. The driveline behaviour is dominated by tuneable nonlinear torsional effects on the second harmonic of the shaft rotation frequency, due to the user-specified Z-configuration of the cardan transmission. These cardan-induced torsional vibrations are more pronounced than unbalance and other effects by design. This is verified by means of preliminary measurements. As a result, this setup will bring significant added value in validating nonlinear model-based virtual sensing methods.

Acknowledgements

The Research Fund KU Leuven and the IWT Flanders within the OPTIWIND project are gratefully acknowledged for their support. This research was also partially supported by Flanders Make, the strategic research centre for the manufacturing industry. This work also benefits from the Belgian Programme on Interuniversity Attraction Poles, initiated by the Belgian Federal Science Policy Office (DYSCO).

Used symbols

- β deflection angle, measured between in- and outgoing shaft of each cardan joint
- $\boldsymbol{d}$ 3x1 zero(-displacement) vector
- $\boldsymbol{f}$ 3x1 bolt pretension force vector
- m pulsating bending moment
- M maximum value of the pulsating bending moment m
- t lateral displacement offset between motor and generator shaft
- T torsional moment

List of tables

References

1. Blockmans, B., Helsen, J., Vanhollebeke, F. and Desmet, W. Dynamic response of a multi-megawatt wind turbine drivetrain under voltage dips using a coupled flexible multibody approach. In ASME 2013 Power Transmission and Gearing Conference, Portland, Oregon, 2013.

2. Amann, N. , Böcker, J. and Prenner, F. Active damping of drive train oscillations for an electrically driven vehicle. IEEE/ASME Trans. Mechatronics, 2004, 9(4), 697-700.

3. Forrier, B., Naets, F. and Desmet, W. Virtual sensing on mechatronic drivetrains using multi-physical models. In Proceedings of the ECCOMAS Thematic Conference on Multibody Dynamics, 2015, 79.

4. Julier, S. J., Uhlmann, J. K. Unscented filtering and nonlinear estimation. Proceedings of the IEEE, 2004, 92(3), 401-422.

5. van der Merwe, R., Wan, E. A., Julier, S. J. Sigma-point Kalman filters for nonlinear estimation and sensor-fusion – applications to integrated navigation. In Proceedings AIAA Guidance, Navigation, and Control Conference, 2004, 16-19.

6. Moschini, S., Gryllias, K., Desmet, W. and Pluymers, B. Virtual sensing for rotor-dynamics. In Proceedings of ASME Turbo Expo 2016, 2016.

7. SKF Group. Rolling bearings. SKF catalogue PUB PU/P1 100000/2 EN, 2013.

8. Schmelz, F., Seherr-Thoss, H.-C., Aucktor, E. Universal joints and driveshafts: analysis, design, applications, Springer-Verlag Berlin Heidelberg GmbH, 2nd edition, 1992, 5–8.

9. Hiller, B., Hübner Elektromaschinen GmbH. Neue Entwicklungen und Anwendungen des Ferraris-Sensors. Seminar: Fortschritte in Regelungs- und Antriebstechnik, Stuttgart, ISW, 2005.

10. Deutsches Institut für Normung. DIN 6885-1:1968-08: Drive type fastenings without taper action – part 1: parallel keys, keyways, deep pattern, Beuth Verlag GmbH, 1968.

11. Voith Turbo GmBH & Co. Universal joint shafts. Voith catalogue G830en, 2013.

12. Wittel, H., Muhs, D., Jannasch, D. and Vossiek, J. Roloff/Matek machine elements, 4rd edition, Academic Service, ISBN 9039523215, 2006.

13. Deutsches Institut für Normung. DIN 3990-1:1987-12: Calculation of load capacity of cylindrical gears – part 1: introduction and general influence factors, Beuth Verlag GmbH, 1987.

14. ISO/TC 108/SC 2. ISO 1940-1:2003 Mechanical vibration – Balance quality requirements for rotors in a constant (rigid) state, 2nd edition, International Organization of Standardization, Geneva, 2003.

15. Heylen, W., Lammens, S. and Sas, P. Modal analysis theory and testing, 2nd edition, KU Leuven, 1998.